One-neutron and noncompound-nucleus decay contributions in the $^{12}C + ^{93}Nb$ reaction at energies near and below the fusion barrier

Sahila Chopra,[1] Manie Bansal,[1] Manoj K. Sharma,[2] and Raj K. Gupta[1]
[1]*Department of Physics, Panjab University, Chandigarh 160014, India*
[2]*School of Physics and Materials Science, Thapar University, Patiala 147004, India*
(Received 30 March 2013; revised manuscript received 31 May 2013; published 30 July 2013)

The dynamical cluster-decay model (DCM), with effects of deformations and orientations of nuclei included in it, is used to study the decay of the hot and rotating compound nucleus $^{105}Ag^*$ formed in a $^{12}C + ^{93}Nb$ reaction at near and below barrier energies. The only parameter of the model is the neck-length parameter, which varies smoothly with the temperature of the compound nucleus, and its value remains within the range of validity ($\sim$2 fm) of the proximity potential. The emissions of both the observed light particles ($A_2 = 1$–4) representing the evaporation residue (ER) and the (energetically favored) intermediate mass fragments (IMFs; $5 \leqslant A_2 \leqslant 13$), together with the so far unobserved fission channel, are considered as the dynamical collective mass motions of preformed fragments or clusters through the barrier. A best fit to data is shown to be obtained only if a large noncompound-nucleus (nCN) contribution, calculated as a quasifission or capture process, is allowed in the DCM. Another interesting result is that the one-neutron contribution is large, rather the largest, when best fits are attempted only for the ER cross sections, but, in turn, it reduces to zero or becomes relatively small if the data on the total fusion cross section σ_{fus}, i.e., $\sigma_{ER} + \sigma_{IMFs}$, are considered. Furthermore, the fusion-fission (ff) cross section σ_{ff}, consisting of symmetric and near-symmetric fragments, at the considered three energies of the experiment, is predicted to be of the order of 10^1 to 10^3 mb, depending on the choice of neck-length parameter for fission region. Further experimental studies are called for both the nCN and ff channels in this reaction.

DOI: 10.1103/PhysRevC.88.014615 PACS number(s): 25.70.Jj, 25.60.Pj, 25.70.Gh, 24.60.Dr

I. INTRODUCTION

Heavy-ion reactions at below barrier energies give rise to highly excited compound nuclear systems that carry large angular momentum and hence decay by emitting multiple light particles (LPs: $A \leqslant 4$, $Z \leqslant 2$, like n, p, and α) or their heavier counterparts and γ rays, termed the evaporation residue (ER), intermediate mass fragments (IMFs) of masses $5 \leqslant A \leqslant 20$ and $2 < Z < 10$, and fusion-fission (ff) consisting of the near symmetric and symmetric fission fragments (nSF and SF, respectively) of masses $(A/2) \pm 20$. In addition, many a times a noncompound-nucleus (nCN) decay process, such as quasifission (qf) or, equivalently, capture, also contribute. The cross section for such a compound nucleus (CN) decay is called the CN production cross section, or simply the (total) fusion cross section σ_{fus}, given as

$$\sigma_{fus} = \sigma_{ER} + \sigma_{IMFs} + \sigma_{ff} + \sigma_{nCN} = \sigma_{CN} + \sigma_{nCN}. \quad (1)$$

In general, the IMFs form a part of the ff and, in a fissionless decay, its contribution is small, of the order of 5 to 10%, i.e., $\sigma_{IMFs} \approx 5$–$10\%\ \sigma_{ER}$. All these components of the fusion cross section are individually measurable quantities. If the σ_{nCN} has not been measured, it can be estimated empirically from the calculated and measured σ_{CN} as

$$\sigma_{nCN} = \sigma_{CN}^{Expt.} - \sigma_{CN}^{Cal.}. \quad (2)$$

It may be pointed out that different mass regions of compound nuclei constitute different combinations of these processes (ER, IMFs, ff, and nCN) or a single one of them as the dominant mode.

In a recent experiment [1], the excitation functions (EFs) of various decay products were measured for the CN $^{105}Ag^*$ formed in a $^{12}C + ^{93}Nb$ reaction at below barrier energies. The observed decay products are the heavy residues whose complementary fragments are the LPs ($A \leqslant 4$) and IMFs ($4 \leqslant A \leqslant 13$). The data are compared with the statistical model code PACE2, which gives the complete fusion (CF, equivalently, ER) cross section consisting of $2n$, $3n$, $4n$, and possibly also ^4H. The disagreement of PACE2 for heavier residues, the IMFs, is taken by the authors as signatures of incomplete fusion (ICF) and/or the direct reaction process, supported by their recoil range distribution measurements. The ICF consists (the complementary fragments) of $^{4,5,6}H$, $^{4,5}He$, ^8Li, $^{9,10,11}Be$, ^{12}B, and ^{13}C. What is striking about the PACE2 predictions is that one-neutron ($1n$) emission is, in general, found missing (cross section $\sigma_{1n} = 0$; see also, e.g., Refs. [2,3] for a $^{64}Ni + ^{100}Mo$ reaction where only the ER cross section is measured [2]). On the other hand, like in Ref. [3], we see in the following that the dynamical cluster-decay model (DCM) [3,4] predicts the contribution due to $1n$ to be the largest, when only the ER cross sections σ_{ER} ($= \sum_{x=1}^{4} \sigma_{xn}$) are considered, but like in experiments [1], in DCM also the σ_{1n} reduces to almost zero (or becomes relatively very small) if the IMFs cross sections σ_{IMFs} (here, IMFs is the summed cross section of 5–13 mass numbers) are also included, i.e., the total fusion cross section σ_{fus} is considered, rather than σ_{ER} alone. It is important to stress that the study of EFs (σ_{fus} as a function of CN excitation energy E_{CN}^*) serves as a powerful tool to understand the reaction mechanism governing the collision dynamics, ranging from CF and ICF to more complex nCN pre-equilibrium or qf processes.

In this paper, we attempt to understand the measured total cross section σ_{Total} ($=\sigma_{ER} + \sigma_{IMFs}$), including the role of missing $1n$ content in σ_{ER}, the fusion-fission σ_{ff} contribution,

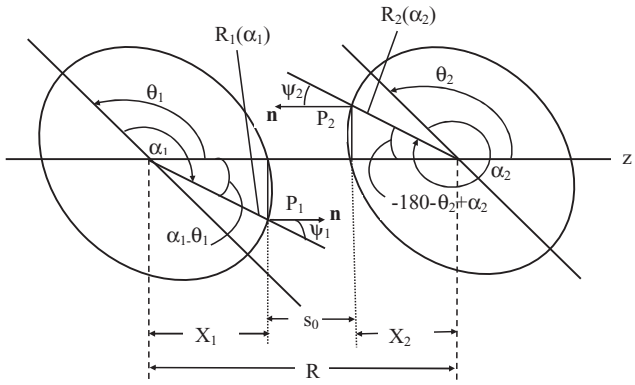

FIG. 1. Schematic configuration of two equal or unequal axially symmetric deformed, oriented nuclei lying in the same plane (azimuthal angle $\Phi = 0^0$) for various θ_1 and θ_2 values in the range 0° to 180°. The θ_i are measured counter-clockwise from the colliding axis and the α_i are measured clockwise from the symmetry axis.

and the $\sigma_{\rm nCN}$ component in $\sigma_{\rm Total}$, together with the EFs for the decay of ^{105}Ag* formed in the ^{12}C + ^{93}Nb reaction, using the DCM [3,4]. We consider the three laboratory energies $E_{\rm Lab.} = 46.4$, 54.0, and 61.2 MeV ($E_{\rm c.m.} = 41.097$, 47.828, and 54.205 MeV, respectively), at which the EFs for $2n$, $3n$ and mass 4 (^{4}H, ^{4}He, and $4n$/^{4}H, respectively) are measured in the present experiment [1]. In the following, we find that, on the basis of the DCM, an unexpectedly large nCN component is predicted in this reaction, whose possibility was pointed out by Mirgule *et al.* [5] in their measured α spectra of the above-noted experiment at near Coulomb barrier energies in the entrance channel. The possible role of deformed configurations is also anticipated in this work [5]. Our DCM calculations include deformation effects up to hexadecapole deformations (β_{2i}, β_{3i}, β_{4i}) with compact orientations θ_{ci}, $i = 1, 2$, of the hot fusion process for the case of coplaner (azimuthal angle $\Phi = 0^\circ$) nuclei (see Fig. 1) [6,7]. For prolate-deformed nuclei, in a compact hot fusion process, the barrier is highest and the interaction radius is smallest in a configuration of belly-to-belly (for $\Phi = 0^\circ$) or equator-cross (for $\Phi \neq 0^\circ$). If one of the nuclei is spherical, the configuration is termed equatorial compact (ec). The presence of large positive hexadeccapole deformation ($\beta_4 \gg 0$), together with $\beta_2 > 0$, results in a not-belly-to-belly compact (nbbc) or not-equatorial compact (nec) configuration, which differs from bbc or ec by as much as 20°. The same is true for oblate-deformed nuclei [8], as illustrated in Table I for the present reaction.

The paper is organized as follows. Section II gives a brief description of the DCM. Our calculations for the ^{12}C + ^{93}Nb reaction, using the DCM, are given in Sec. III. A summary and conclusions of our work are presented in Sec. IV. Brief reports of this work have been reported at the 2012 Department of Atomic Energy (DAE) Symposium on Nuclear Physics [12] and the 2013 Chandigarh Science Congress (CHASCON) [13].

II. THE DYNAMICAL CLUSTER-DECAY MODEL (DCM)

The DCM of Gupta and collaborators [3,4] is based on collective coordinates of mass (and charge) asymmetries η (and η_Z) [$\eta = (A_1 - A_2)/(A_1 + A_2)$, $\eta_Z = (Z_1 - Z_2)/(Z_1 + Z_2)$] and relative separation R, with multipole deformations $\beta_{\lambda i}$ ($\lambda = 2, 3, 4$; $i = 1, 2$) and orientations θ_i. In terms of these coordinates, for the CN fusion probability in the entrance channel taken as unity for all partial waves (an assumption more suitable for higher energies, but extended here to lower energies), we define the CN decay cross section for ℓ partial

TABLE I. The compact orientations θ_{ci}, as per the prescription in Ref. [7], the deformations (β_{2i}, β_{3i}, β_{4i}; $i = 1, 2$) from Refs. [9,10], and the barrier height and position, V_B and R_B, calculated at $\ell = 0$ and $T = 0$ for target-projectile combinations (A_1, A_2) referring to minima in mass fragmentation potential $V(A_i)$, for compact hot configurations. β_{22} for $A_2 < 16$ and $Z_2 < 8$ are from the relativistic mean-field calculations [11]. θ_{ci} are independent of ℓ values. V_B increases and R_B changes as the ℓ value increases. For example, for ^{104}Ag + $1n$ at $\ell_{\rm max} = 75\,\hbar$, $V_B = 97.60$ MeV, and $R_B = 9.50$ fm. For $A_2 = 4$, the cases of ^{4}H and ^{4}He are also included.

Reactions ($A_1 + A_2$)	Deformations of (A_1, A_2)						Barriers		Compact	
	β_{21}	β_{31}	β_{41}	β_{22}	β_{32}	β_{42}	V_B	R_B	θ_{c1}	θ_{c2}
^{104}Ag + $1n$	0.153	0.0	0.001	0.0	0.0	0.0	0	14.939	90°	*s*
^{103}Ag + $2n$	0.134	0.0	0.016	0.0	0.0	0.0	0	15.208	90°	*s*
^{102}Ag + $3n$	0.125	0.0	0.022	0.0	0.0	0.0	0	15.418	90°	*s*
^{101}Ag + $4n$	0.08	0.0	0.018	0.0	0.0	0.0	0	15.644	90°	*s*
^{101}Pd + ^{4}H	0.134	0.0	0.032	0.0	0.0	0.0	5.81	10.496	90°	*s*
^{101}Rh + ^{4}He	0.152	0.0	0.025	0.125	0.0	0.0	12.021	9.879	90°	106°
^{100}Pd + ^{5}H	0.088	0.0	0.019	0.0	0.0	0.0	5.71	10.744	90°	*s*
^{99}Ru + ^{6}Li	0.152	0.0	0.034	−0.099	0.0	0.0	17.7	9.847	90°	178°
^{98}Ru + ^{7}Li	0.115	0.0	0.038	−0.086	0.0	0.0	17.423	10.043	90°	172°
^{97}Ru + ^{8}Li	0.053	0.0	0.001	−0.09	0.0	0.0	17.203	10.196	90°	174°
^{96}Tc + ^{9}Be	0.053	0.0	0.001	−0.107	0.0	0.0	22.7	10.069	90°	172°
^{95}Mo + ^{10}B	0.053	0.0	0.001	−0.121	0.0	0.0	27.981	9.948	88°	180°
^{94}Mo + ^{11}B	0.053	0.0	0.001	−0.086	0.0	0.0	27.705	10.069	88°	172°
^{93}Mo + ^{12}B	0.053	0.0	0.009	−0.028	0.0	0.0	27.44	10.189	90°	180°
^{92}Nb + ^{13}C	0.053	0.0	0.017	−0.02	0.0	0.0	32.278	10.143	80°	180°

waves as

$$\sigma = \frac{\pi}{k^2}\sum_{\ell=0}^{\ell_{\max}}(2\ell+1)P_0P, \quad k=\sqrt{\frac{2\mu E_{\rm c.m.}}{\hbar^2}}, \tag{3}$$

where P_0 is the preformation probability referring to η motion and P is the penetrability, to R motion, both dependent on angular momentum ℓ and temperature T. μ is the reduced mass with m being the nucleon mass. $\ell_{\max}$ is the maximum angular momentum, defined for the light particle ER cross section $\sigma_{\rm ER}(\ell)\to 0$, equivalently, $P_0(\ell)\to 0$ (with limiting value $P_0 > 10^{-10}$, as shown in Fig. 5). The same formula is applicable to the nCN decay process, calculated here as the qf decay channel or, equivalently, the capture process where $P_0 = 1$ for the *incoming channel* because, for qf, the target and projectile nuclei can be considered to have not yet lost their identity. In other words, no mass distribution takes place in qf or the capture process, and the DCM reduces to an (ℓ-summed) extended-Wong model [14].

P_0 is the solution of the stationary Schrödinger equation in η, at a fixed $R = R_a$,

$$\left\{-\frac{\hbar^2}{2\sqrt{B_{\eta\eta}}}\frac{\partial}{\partial\eta}\frac{1}{\sqrt{B_{\eta\eta}}}\frac{\partial}{\partial\eta}+V(R,\eta,T)\right\}\psi^{\nu}(\eta)=E^{\nu}\psi^{\nu}(\eta), \tag{4}$$

with $\nu = 0, 1, 2, 3\ldots$ referring to ground-state ($\nu = 0$) and excited-state solutions. Then, the probability

$$P_0(A_i) = |\psi[\eta(A_i)]|^2\sqrt{B_{\eta\eta}}\frac{2}{A}, \tag{5}$$

where, for a Boltzmann-like function,

$$|\psi|^2 = \sum_{\nu=0}^{\infty}|\psi^{\nu}|^2\exp(-E^{\nu}/T). \tag{6}$$

For the position $R = R_a$, the first turning point for calculating the penetration P, in the decay of a hot CN, we use the following postulate [15–17],

$$\begin{aligned} R_a(T) &= R_1(\alpha_1,T)+R_2(\alpha_2,T)+\Delta R(T),\\ &= R_t(\alpha,\eta,T)+\Delta R(T), \end{aligned} \tag{7}$$

with radius vectors

$$R_i(\alpha_i,T) = R_{0i}(T)\left[1+\sum_{\lambda}\beta_{\lambda i}Y_{\lambda}^{(0)}(\alpha_i)\right], \tag{8}$$

with temperature-dependent nuclear radii $R_{0i}(T)$ for the equivalent spherical nuclei [18],

$$R_{0i} = \left[1.28A_i^{1/3}-0.76+0.8A_i^{-1/3}\right](1+0.0007T^2). \tag{9}$$

Note that in Eq. (7) the only parameter of the model is $\Delta R(T)$, the neck-length parameter, or equivalently the first turning point $R_a(T)$, where both ΔR and R_a are T dependent, with the η dependence contained only in R_t. $\Delta R(T)$ assimilates the deformation and neck formation effects between two nuclei, introduced within the extended model of Gupta and collaborators [19–21]. This method of introducing the neck-length parameter ΔR is similar to that used in both the scission-point [22] and saddle-point [23,24] statistical fission models.

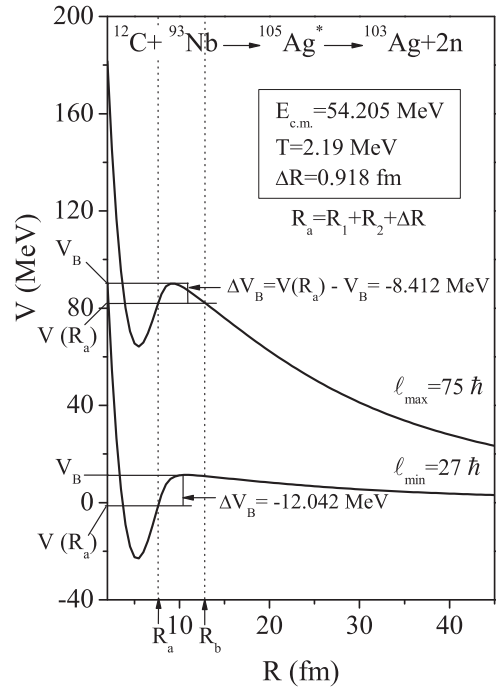

FIG. 2. The ℓ-dependent scattering potential $V(R)$ for ^{103}Ag + $2n$, in the decay of ^{105}Ag* formed in the ^{12}C + ^{93}Nb reaction at $E_{\rm c.m.} = 54.205$ MeV. The concept of barrier lowering $\Delta V_B = V(R_a) - V_B$ is also shown in this figure for both the $\ell_{\max} = 75\ \hbar$ and $\ell_{\min} = 27\ \hbar$ values. The first and second turning points R_a and R_b are also labeled.

Also, we use the Süsmann central radii $C_i = R_i - b^2/R_i$ (in fm), where the surface thickness parameter (in fm) [18] is

$$b(T) = 0.99(1+0.009T^2). \tag{10}$$

The choice of parameter R_a (equivalently, ΔR) in Eq. (7), for a best fit to the data, allows us to relate in a simple way the $V(R_a,\ell)$ to the top of the barrier $V_B(\ell)$ for each ℓ, by defining their difference $\Delta V_B(\ell)$ as the effective "lowering of the barrier":

$$\Delta V_B(\ell) = V(R_a,\ell) - V_B(\ell). \tag{11}$$

Note, ΔV_B for each ℓ is defined as a negative quantity because the actually used barrier is effectively lowered. This is illustrated in Fig. 2 for $\ell_{\min}$ and $\ell_{\max}$ values, whose values are fixed for the LPs' (here, e.g., xn, x = 1–4) cross section $\sigma_{xn}(\ell)\to 0$ (or the penetrability starts to contribute, i.e., $P_0 > 10^{-10}$ and $P > 10^{-15}$ for the example studied; see, Figs. 5 and 6, respectively). Thus, the fitted parameter ΔR controls the "barrier lowering" ΔV_B.

The collective fragmentation potential $V(R,\eta,T)$ in Eq. (4), which brings the structure effects of the CN into the formalism, is calculated according to the Strutinsky renormalization procedure ($B = V_{\rm LDM} + \delta U$), using the T-dependent liquid-drop-model energy $V_{\rm LDM}(T)$ of Davidson *et al.* [25], and the "empirical" shell corrections δU of Myers and Swiatecki [26], for spherical nuclei, also made T dependent to vanish exponentially with $T_0 = 1.5$ MeV [27]. Then, including also the T dependence in the nuclear proximity V_P, the Coulomb V_C, and the ℓ-dependent

potential V_ℓ,

$$V_R(\eta, T) = \sum_{i=1}^{2}[V_{\rm LDM}(A_i, Z_i, T)] + \sum_{i=1}^{2}[\delta U_i]\exp\left(-\frac{T^2}{T_0^2}\right) + V_P(R, A_i, \beta_{\lambda i}, \theta_i, \Phi, T) + V_C(R, Z_i, \beta_{\lambda i}, \theta_i, \Phi, T) + V_\ell(R, A_i, \beta_{\lambda i}, \theta_i, \Phi, T), \quad (12)$$

where V_P, V_C, and V_ℓ are for deformed oriented nuclei. The moment of inertia used in V_ℓ is in the complete sticking limit, $I_S(T) = \mu R^2 + \frac{2}{5}A_1 m R_1^2(\alpha_1, T) + \frac{2}{5}A_2 m R_2^2(\alpha_2, T)$. In general, the experimental numbers for ℓ are based on the moment of inertia calculated in the nonsticking limit $I = I_{\rm NS} = \mu R^2$. This use of reduced mass alone corresponds to the supposition of prompt emission of fragments. However, I_S is more appropriate for the proximity potential (nuclear surfaces $\leqslant$2 fm apart) which has consequences for the limiting ℓ value to be much larger due to the relatively larger magnitude of I_S. This is shown [28,29] to result in the reduction of the nuclear surface separation distance ΔR, and vice versa for $I_{\rm NS}$.

The same considerations are applied to neutron and proton clusters of x ($\geqslant$1) nucleons, by defining [30,31] the binding energy of a cluster with x neutrons as x times the binding energy of one neutron (equivalently, the mass excess Δm_n = 8.0713 MeV), i.e.,

$$B(A_L = xn) = x\Delta m_n,$$

and defining the same for proton clusters as

$$B(A_L = xp) = x\Delta m_p - a_c A_L^{5/3},$$

with $\Delta m_p = 7.2880$ MeV, the one-proton mass excess or equivalently the binding energy of one proton. a_c = 0.7053 MeV [26], with the additional term due to a_c acting as the disruptive Coulomb energy [$= -a_c(Z_L^2/A_L^{1/3})$] between the x protons (here $x = A_L = Z_L$). Because it is difficult to define the volume and the surface of n or p clusters, the T dependence of their binding energy is included only via the shell correction term δU, and not in $V_{\rm LDM}$. The above definitions of n or p clusters are found to describe well the "halo" structures of almost all the n- or p-rich light nuclei [30,31] and mean that the nucleons in these clusters are taken to be unbound (i.e., structureless particles), following the model of Hansen and Jonson [32], the few-body theories [33], or as suggested by some experiments [34,35].

The mass parameters $B_{\eta\eta}$, entering Eq. (4) for P_0 calculations, are the smooth classical hydrodynamical masses [36], because at large T values the shell effects are almost completely washed out. For smaller T (<1.5 MeV), in principle, the shell-corrected masses, like the Cranking masses, should be used, but for simplicity we use the same smooth classical hydrodynamical masses.

The penetrability P in Eq. (3) is the WKB integral,

$$P = \exp\left(-\frac{2}{\hbar}\int_{R_a}^{R_b}\{2\mu[V(R,T) - Q_{\rm eff}]\}^{1/2}dR\right), \quad (13)$$

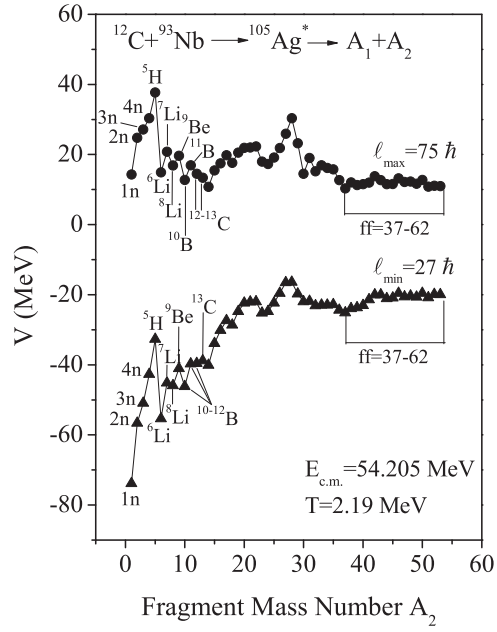

FIG. 3. Mass fragmentation potential minimized in charge coordinate η_Z for the decay of ^{105}Ag* formed in the ^{12}C + ^{93}Nb reaction at $E_{\rm c.m.}$ = 54.21 MeV and at $\ell_{\rm min}$ and $\ell_{\rm max}$ values. For mass $A_2 = 4$, the minimized fragment is ^{4}H, but is here replaced by the corresponding binding energy of 4n. The neck-length parameters ΔR are given in Table II and refer here to Cal.2, the case of both ER and IMFs fitted. For fragments $A_2 > 13$, ΔR is same as that for IMFs.

solved analytically [37,38], with the second turning point R_b (see Fig. 2) satisfying

$$V(R_a) = V(R_b) = Q_{\rm eff} = {\rm TKE}(T). \quad (14)$$

As the ℓ value increases, the $Q_{\rm eff}(T)$ [=TKE(T), total kinetic energy]increases and hence $V(R_a, \ell)$ increases. Thus, R_a acts like a parameter through $\Delta R(T)$, and we define that R_a is the same for all ℓ values, i.e., $V(R_a) = Q_{\rm eff}(T, \ell = 0)$. This is required because we do not know how to add the ℓ effects in binding energies. Alternatively, we may define R_a and hence

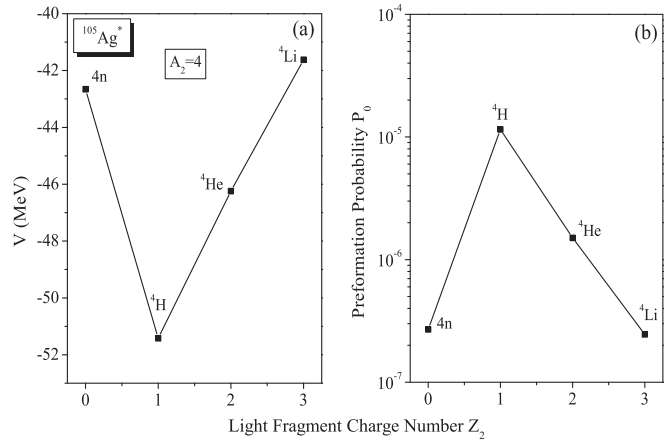

FIG. 4. Same as for Fig. 3, but for charge fragmentation potential $V(\eta_{Z_2})$ and preformation factor $P_0(\eta_{Z_2})$ for mass $A_2 = 4$ fragment at $\ell_{\rm min}$ value.

TABLE II. Calculated fusion-evaporation cross sections $\sigma_{ER}^{Cal.1}$ due to LPs alone (referred to as Cal.1), compared with the corresponding experimental data $\sigma_{ER}^{Expt.}$ of Ref. [1]. Also tabulated are the calculated cross sections $\sigma_{ER,IMFs}^{Cal.2}$ due to both LPs and IMFs taken together for a best fit (referred to as Cal.2) and compared with the measured fusion cross section $\sigma_{fus}^{Expt.}$. Also σ_{qf} is calculated and added to both σ_{ER} and σ_{IMFs} (referred to as Cal.3), giving the $\sigma_{fus}^{Cal.}$. Here LPs and IMFs refer, respectively, to $A_2 = 1n$–$3n$, ^{4}H, ^{4}He or $4n$, and a *sum* of $A_2 = 5$–13. The neck-length parameter ΔR for LPs and IMFs are considered to take different values in Fig. 3 for the best fit to data, in each case of ^{4}H, ^{4}He, or $4n$ for mass 4 fragment. The variation of ΔR with T ($\equiv E_{c.m.}$) or fragment mass (here LPs) is found to be not as smooth as expected because the nCN ($\equiv$qf) component being large has been a difficult task to separate out. The cross sections marked with † in Cal.3 should, in principle, be zero by the definition of the nCN contribution.

Decay channel	DCM-Cal.1 (ER alone)			DCM-Cal.2 (Both ER and IMFs)			DCM-Cal.3 (qf contribution)		
	ΔR (fm)	$\sigma_{ER}^{Cal.1}$ (mb)	$\sigma_{ER}^{Expt.}$ (mb)	ΔR (fm)	$\sigma_{ER,IMFs}^{Cal.2}$ (mb)	$\sigma_{fus}^{Expt.}$ (mb)	ΔR (fm)	σ_{qf} (mb)	$\sigma_{fus}^{Cal.}$ (mb)
$E_{c.m.} = 54.205$ MeV					ER: $1n$, $2n$, $3n$, and $4n$				
$1n$	1.363	75.4	0	0.8	0.587	0	0.5	0.137	0.724
$2n$	1.363	7.6	7.6 ± 1.4	1.803	7.6	7.6 ± 1.4	0.2	0.002†	7.602
$3n$	1.363	0.156	398.2 ± 46.9	1.5	0.11	398.2 ± 46.9	1.3695	398	398.11
$4n$	1.363	0.0022	203.4 ± 26.4	1.5	0.0024	203.4 ± 26.4	1.3345	203	203.0024
IMFs (5–13)	–	–	–	1.5	215	296.4	0.9099	79.9	294.9
$E_{c.m.} = 54.205$ MeV					ER: $1n$, $2n$, $3n$, and ^{4}H				
$1n$	1.3847	81	0	0.79	0.533	0	0.5	0.137	0.670
$2n$	1.3847	7.67	7.6 ± 1.4	1.81	7.6	7.6 ± 1.4	0.3	0.0062†	7.606
$3n$	1.3847	0.185	398.2 ± 46.9	1.99	0.398	398.2 ± 46.9	1.3691	397	397.398
^{4}H	1.3847	2.51	233.7 ± 25.7	1.99	1.43	233.7 ± 25.7	1.201	232	233.43
IMFs (5–13)	–	–	–	1.55	249	296.4	0.8379	47.2	296.2
$E_{c.m.} = 47.828$ MeV					ER: $1n$, $2n$, $3n$, and ^{4}He				
$1n$	1.571	455	0	1.15	9.98	0	0.3	0.003	9.983
$2n$	1.571	38.2	38.2 ± 3.9	1.75	14.7	38.2 ± 3.9	1.028	23.4	38.1
$3n$	1.571	0.63	615.4 ± 125.3	0.31	0.0001	615.4 ± 125.3	1.4212	614	614.0001
^{4}He	1.571	0.067	2.8 ± 0.4	1.843	2.80	2.8 ± 0.4	0.1	0.049†	2.849
IMFs (5–13)	–	–	–	1.513	168	168	0.1	0.01†	168.01
$E_{c.m.} = 41.097$ MeV					ER: $1n$, $2n$, $3n$, and ^{4}H				
$1n$	1.2586	38.2	0	1.0	4.84	0	0.3	0.012	4.852
$2n$	1.2586	2.69	80.0 ± 9.6	1.9	13.2	80.0 ± 9.6	1.1272	66.6	79.8
$3n$	1.2586	0.04	260.3 ± 11.3	1.9	0.508	260.3 ± 11.3	1.2994	259	259.508
^{4}H	1.2586	1.8	1.8 ± 0.3	1.4672	1.8	1.8 ± 0.3	0.4	0.007†	1.807
IMFs (5–13)	–	–	–	1.3528	28	28	0.3	0.074†	28.074

$\Delta R(T)$ in terms of the T-dependent binding energies $B(T)$ as

$$Q_{eff}(T) = B(T) - [B_1(T=0) + B_2(T=0)] = \text{TKE}(T) = V[R_a(T)]. \quad (15)$$

Here B's are the respective binding energies for the decay of hot CN at temperature T to two exit-channel fragments observed in the ground state (g.s.; $T = 0$). Equation (15) could apparently be achieved only by emitting some LPs, like n, p, and α or γ rays, of energy:

$$E_x = B(T) - B(0) = Q_{eff}(T) - Q_{out}(T=0) = \text{TKE}(T) - \text{TKE}(T=0), \quad (16)$$

which is zero for the g.s. ($T = 0$) decay, the case of exotic cluster radioactivity, treated within the preformed cluster model [37,38].

Apparently, Eq. (16) with respect to Eq. (15) suggests that the emission of LPs starts early in the decay process. The exit channel fragments in Eq. (15) are then obtained in the ground state with TKE($T = 0$), as can be seen by calculating $E^*_{CN} - E_x$:

$$E^*_{CN} - E_x = |Q_{out}(T)| + \text{TKE}(T=0) + \text{TXE}(T), \quad (17)$$

where the total excitation energy TXE(T) is used in, *not treated here*, the secondary emission of LPs from the fragments which are otherwise in their ground states with TKE($T = 0$) in the radial motion. Instead, we compare the present calculations with the, in general, available primary pre-secondary-evaporation fragment emission data [24,39]. Thus, by defining $Q_{eff}(T)$ as above, via the T-dependent binding energies [Eq. (15)], the DCM becomes a parameter free [40], nonstatistical, dynamical treatment of the complete decay of hot and rotating CNs, where the LPs emission are treated on par with the IMFs and ff decays.

III. CALCULATIONS AND RESULTS

In this section, we present our calculations for the possible decay processes of ^{105}Ag* formed in the ^{12}C + ^{93}Nb reaction at different center-of-mass energies $E_{c.m.}$. As noted in the

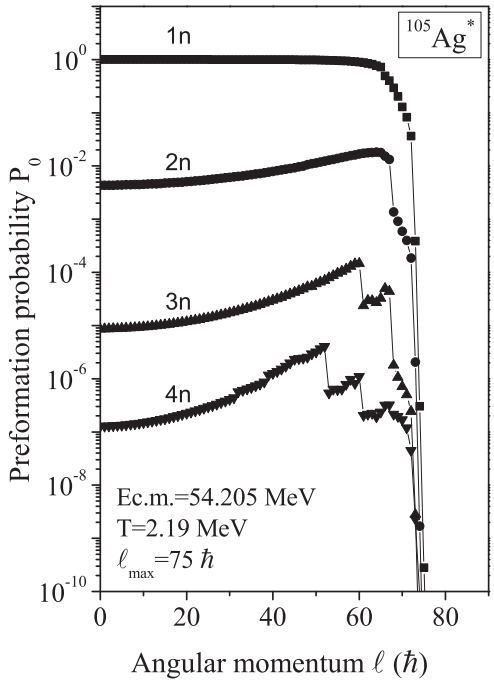

FIG. 5. Preformation probability P_0 as a function of angular momentum ℓ for xn decays of ^{105}Ag* formed in the $^{12}C + ^{93}Nb$ reaction at $E_{c.m.} = 54.205$ MeV. $P_0 \sim 10^{-10}$ for $\ell_{max} = 75\,\hbar$.

Introduction, in this reaction, the experimentally observed decay channels of ER are $2n$-$4n$, or $2n$, $3n$, and ^{4}H, populated by CF, and the intermediate mass fragments (IMFs) $A_2 = 5$–13, considered as the ICF products. In the following, we treat both the observed cases of ER and IMFs, together with the not yet observed ff component, as the CF products, i.e., due to the

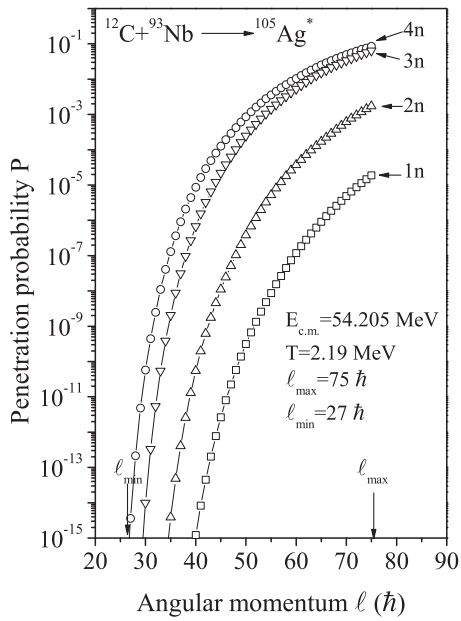

FIG. 6. Penetration probability P as a function of angular momentum ℓ for xn decays of ^{105}Ag* formed in the $^{12}C + ^{93}Nb$ reaction at $E_{c.m.} = 54.205$ MeV, calculated up to $\ell_{max} = 75\,\hbar$. $P \sim 10^{-15}$ for $\ell_{min} = 27\,\hbar$.

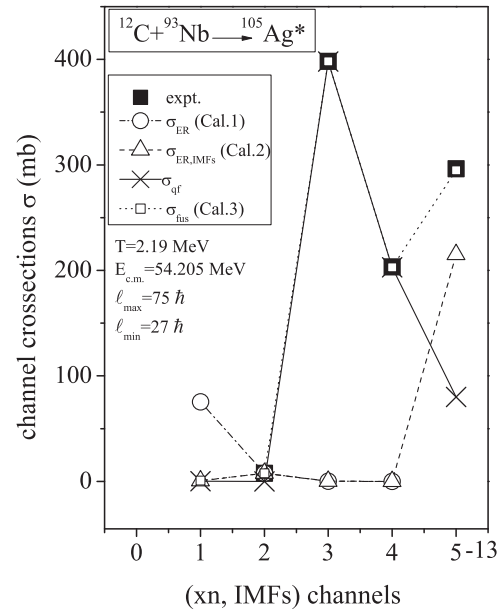

FIG. 7. Calculated fusion ER and (sum of) IMFs cross sections, σ_{ER} and σ_{IMFs}, for decay of ^{105}Ag* formed in the $^{12}C + ^{93}Nb$ reaction, compared with experimental data at $E_{c.m.} = 54.205$ MeV. $\ell_{max} = 75\,\hbar$ and $\ell_{min} = 27\,\hbar$. Cal.1 (open circles) refers to fitting of ER alone, and Cal.2 (up triangles) refers to both ERs and IMFs fitted together. Cal.3 (crosses) gives the noncompound, qf contribution, which upon adding to σ_{ER} and σ_{IMFs} gives the calculated fusion cross section $\sigma_{fus}^{Cal.}$ (open squares), compared with the experimental value (solid squares) $\sigma_{fus}^{Expt.}$.

decay of the CN. Then, the ER ($A \leqslant 4$) should also constitute the $2n$, $3n$, and ^{4}He. Furthermore, the $1n$ evaporation channel, not observed in the experiment, is treated on equal footing. The nCN effects, if any, are considered to be due to qf or the capture process where the preformation factor $P_0 = 1$ for the incoming nuclei to keep their identity.

Figure 3 shows the calculated mass fragmentation potential $V(A_2)$ for the best-fitted ΔR to both the measured ER and the summed IMFs cross sections at $E_{c.m.} = 54.205$ MeV ($T = 2.19$ MeV) and at ℓ_{min} and ℓ_{max} values. For fragments heavier than the IMFs, ΔR is same as that for the IMFs. Though ^{4}H is energetically the most favored (see, Fig. 4 where the charge dispersion potential $V(Z_2)$ and the corresponding preformation factor $P_0(Z_2)$ is plotted for the mass $A_2 = 4$ case), in Fig. 3 we have replaced it by the binding energy of $4n$ (and the complementary heavy fragment). Note that some fragments change in going from the ℓ_{min} to the ℓ_{max} value. ΔR is taken different for each decay channel of ER and the summed-IMFs, as given in Table II (refer to Cal.2, the case of both ER and IMFs fitted). A similar procedure is carried out for ^{4}H and ^{4}He fragments, replacing $4n$ (see Table II for each case of $4n$, ^{4}H, and ^{4}He occurring at different $E_{c.m.}$'s). Other characteristic properties for nuclei referring to ER and IMFs are given in Table I for the $\ell = 0$ case. The cases of ^{4}H and ^{4}He, in place of $4n$, are also included in Table I. We notice in Table I that, except for one prolate-deformed + prolate-deformed configuration (^{101}Rh + ^{4}He), other configurations are of either prolate-deformed + spherical nuclei or prolate-deformed + oblate-deformed nuclei, and, due to

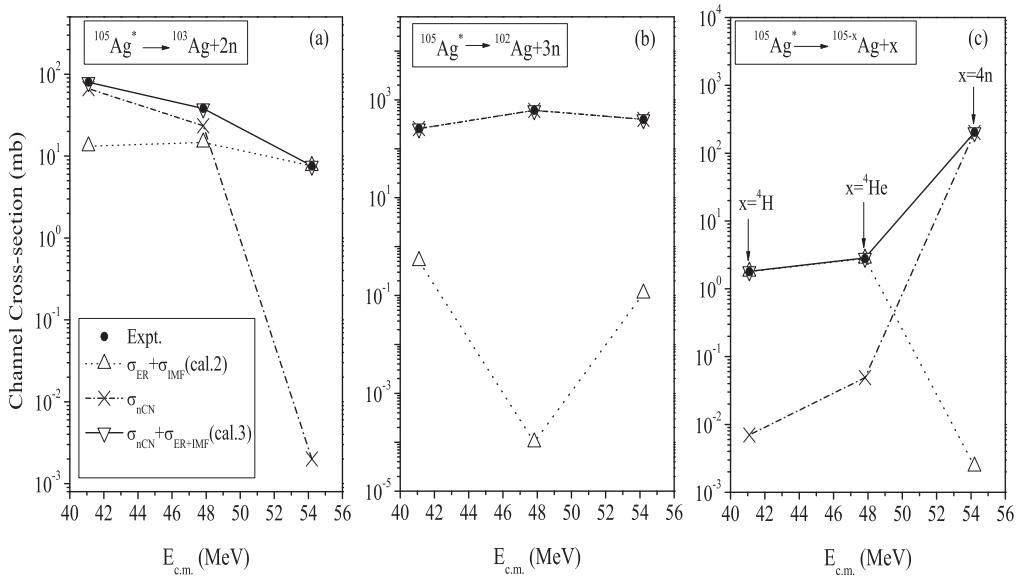

FIG. 8. Calculated excitation functions (EFs) compared with experimental data for (a) $2n$, (b) $3n$, and (c) mass 4 emission in the decay of $^{105}Ag^{*}$ formed in the $^{12}C + {}^{93}Nb$ reaction. Calculations are shown for σ_{ER+IMF} (up triangle), σ_{nCN} (crosses), and the total $\sigma_{ER+IMF+ncN}$ (down triangle).

the positive β_{41}, the compact orientations θ_{ci} are affected by as much as 16° (for the prolate-deformed case 90° changes to 106° or 80° and for the oblate-deformed case 180° goes to 172°), meaning thereby that higher-order deformations (β_4) play an important role for the orientation degree of freedom.

The calculated P_0 and P, as a function of ℓ, based on $V(\eta)$ of Fig. 3 and $V(R)$ like that of Fig. 2, respectively, are plotted in Figs. 5 and 6 for the illustrative ER channels. These figures fix the ℓ_{max} and ℓ_{min} values, respectively, where the contributions to cross sections become negligible. Interesting enough, the $1n$ channel competes with the other three neutron channels. In fact, the $1n$ product is not only the most strongly preformed product (largest P_0) but also has large penetrability P, which however is smaller than for the other three neutron channels. In other words, the σ_{1n} makes the largest contribution to the ER cross section $\sigma_{ER} = \sum_{x=1}^{4} \sigma_{xn}$, if we fit only the ER data (see Fig. 7 and Table II). Figure 7 (open circles) and Table II (top pannel, cal.1) show that only σ_{2n} is best fitted, with a large σ_{1n} value of 75.4 mb (compared to zero in experiments), whereas σ_{3n} and σ_{4n} are very small (=0.156 and 0.0022 mb), compared to measured values of 398.2 ± 46.9 and 203.4 ± 26.4 mb, respectively. Note that different ΔR values are used for different xn channels, which means different reaction times for different residue products. On the other hand, if we also include the IMFs (here the sum of $A_2 = 5$–13 cross sections) in the fitting of ΔR, i.e., both ER and IMFs are fitted together (Cal.2 in Table II and up triangles in Fig. 7), then for the same best fit of σ_{2n}, and σ_{IMFs} close to experiments (with in ∼75% of the data at this highest energy), σ_{1n} reduces nearly to zero, as required by experiments, but the σ_{3n} and σ_{4n} are still very small compared to data and call for large noncompound (qf or capture) contributions. Following Eq. (2), we define the nCN component as the order of disagreement, i.e., the difference between the calculated and the measured decay cross sections:

$$\sigma_{\mathrm{nCN}} = \sigma^{\mathrm{expt}}_{\mathrm{decay\text{-}product}} - \sigma^{\mathrm{cal}}_{\mathrm{decay\text{-}product}}.$$

Then, with the proper choice of ΔR for each decay product, i.e., within the nuclear proximity limit of ∼2 fm, an exact fit to data for both the ER and IMFs cross sections is obtained. Note that such a large nCN component is perhaps predicted for the first time.

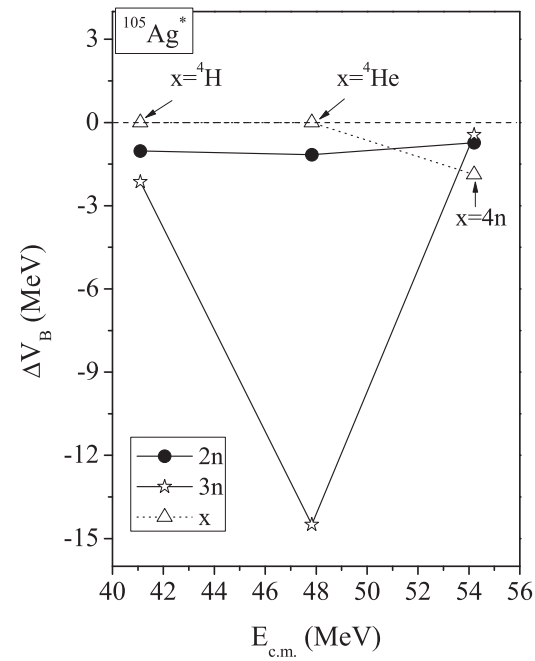

FIG. 9. The barrier lowering ΔV_B, defined by Eq. (11), as a function of $E_{c.m.}$ for the case of $\ell = \ell_{max}$ in the decay of $^{105}Ag^{*}$ formed in the $^{12}C + {}^{93}Nb$ reaction.

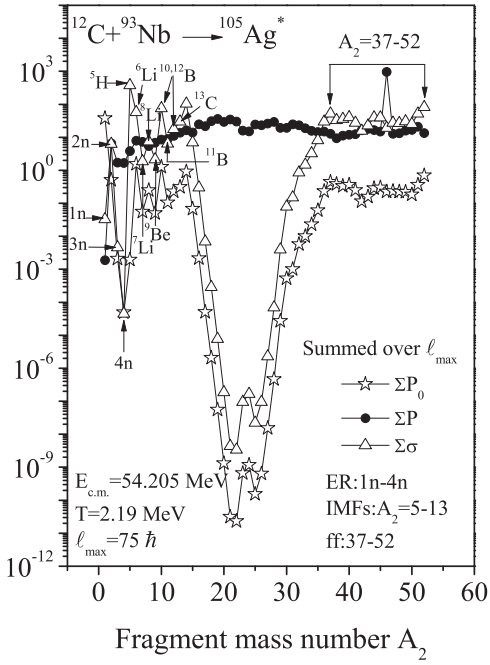

FIG. 10. The ℓ-summed fragment preformation probability P_0, the penetrability P, and the decay cross section σ as a function of the light fragment mass number A_2 for the compound system ^{105}Ag* formed in the ^{12}C + ^{93}Nb reaction at $E_{c.m.} = 54.205$ MeV, $\ell_{max} = 75\,\hbar$. For $A_2 > 13$ fragments $\Delta R = 1.5$ fm, the same as that for IMFs.

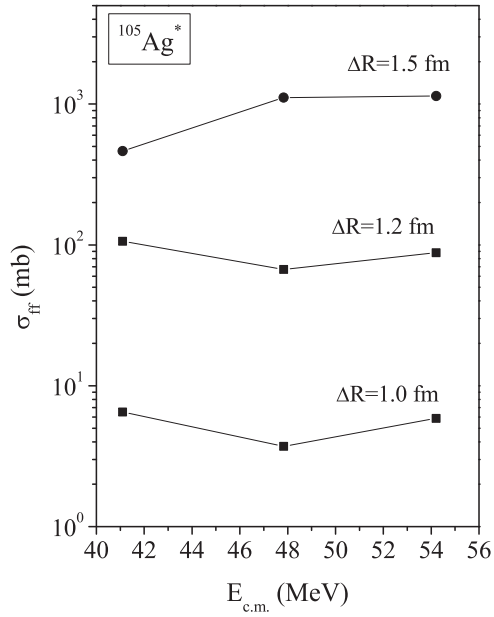

FIG. 11. Calculated fusion-fission cross section σ_{ff} for the decay of ^{105}Ag* formed in the ^{12}C + ^{93}Nb reaction as a function of center-of-mass energy $E_{c.m.}$. Here ff is defined as the mass window $A_2 = 37$–52 plus their complementary heavy fragments $A_1 = 68$–53.

Table II (and Fig. 7) shows that the largest nCN content is in $3n$ emission, and the $2n$, mass 4 (^{4}H and ^{4}He), and IMFs are dominantly the CN decays. This is further shown in Fig. 8 where the EFs are plotted for the emission of $2n$, $3n$, and mass 4 fragments. We notice that whereas the CN and nCN components are comparable in $2n$ and mass 4 decays, the $3n$ is shown to be mainly a nCN decay [Fig. 8(b)] at the three considered excitation (or c.m.) energies. This could perhaps be further understood in terms of the "barrier lowering" parameter ΔV_B, shown in Fig. 9 as a function of $E_{c.m.}$. Apparently, the largest barrier lowering is required for $3n$ emission, and more so at $E_{c.m.} = 47.83$ MeV. ΔV_B is nearly zero for mass 4 and very small for $2n$ emission. Thus, nuclear force(s) other than the proximity force used here could be more relevant to the reaction under study [41].

Figure 10 shows our calculated ℓ-summed P_0, P, and σ as functions of the light mass fragment A_2 for $E_{c.m.} =$ 54.205 MeV. We notice from this figure that, in addition to the observed ER and IMFs decay products, the IMF window is extended up to $A_2 \approx 18$ (cross sections of similar order as for the observed ER and IMFs) and a new window of symmetric and near-symmetric fission of fragment masses $(A/2)\pm16$, i.e., of $A_2 = 37$–52 and complementary heavy fragments, is evident whose yields (P_0 and/or σ) are as large as those for the observed IMFs and LPs. Defining σ_{ff} as the sum of cross sections for $A_2 = 37$–52 and complementary heavy fragments, we notice from Fig. 11 that the fission component is significantly large, of the order of 10^3 mb. Note that in this case $\Delta R = 1.5$ fm for the fission region, the same as that for IMFs and $3n$, but larger than that for $2n$ emission. Knowing that ΔR for ff is much smaller than that for ER [42] (LPs are promptly emitted particles, and hence with larger ΔR), we have varied ΔR for the ff region and recalculated σ_{ff} for $\Delta R = 1$ and 1.2 fm. This is also plotted in Fig. 11. The interesting result is that σ_{ff} is of the order of 10^1 to 10^3 mb, depending on the choice of the neck-length parameter ΔR for the fission region. Thus, experimental measurements of σ_{ff} are called for in this reaction.

IV. SUMMARY AND CONCLUSIONS

Concluding, we have applied the DCM to the decay of ^{105}Ag* at near and below barrier energies in order to study the missing contribution of $1n$ in ER cross sections and the nCN, qf contribution required in fitting the observed EFs for both the ER and the IMFs. The model contains deformation effects up to hexadecapole for coplanar nuclei with compact orientations of the hot fusion process. The neck-length ΔR, which itself varies smoothly with the excitation energy or temperature T of the system, is the only parameter of the model whose value always stays within the proximity limit of ~2 fm.

It is shown for the first time that if ER data alone are considered, fits are possible only for the $2n$ cross section, predicting a rather large contribution of $1n$ (compared to zero for experiments) and a strong underestimation of both $3n$ and $4n$ (or ^{4}H) cross sections. However, if the fitting of both the ER and the IMFs (only the sum of cross sections in this later case) is done simultaneously, interestingly σ_{1n} reduces nearly to zero (at least becomes comparatively very small), to be compared with zero of experiments, for a similar best fit to $2n$ or ^{4}H cross-section data, and σ_{IMFs} also obtained close to data, at least for the higher energies. Other ER channel

cross sections are still very small compared to experiments, which suggests a large nCN, qf contribution. Once the nCN, qf component is included, the data for both the ER and the IMFs, i.e., total EFs, are fitted nearly exactly. The nCN component obtained is rather large, a case perhaps noted for the first time. Furthermore, different ΔR are used for different ER and IMF channels, which refers to different reaction times for different residue products.

Furthermore, our calculations suggest a significant ff component, which constitutes an extended IMF window plus a symmetric and nearly symmetric fission mass component. Apparently, further experiments are needed not only for the measurement of nCN effects but also for the fission component.

ACKNOWLEDGMENTS

This work was supported partially by the Department of Science & Technology (DST), Government of India. A part of the computations for this work were performed on the CAS-FIST-PURSE High Performance Computing Cluster (HPCC) at the Physics Department, Panjab University, Chandigarh, India.

[1] T. Ahmad, I. A. Rizvi, A. Agarwal, R. Kumar, K. S. Golda, and A. K. Chaubey, Int. J. Mod. Phys. E **20**, 645 (2011).
[2] M. L. Halbert *et al*., Phys. Rev. C **40**, 2558 (1989).
[3] S. K. Arun, R. Kumar, and R. K. Gupta, J. Phys. G: Nucl. Part. Phys. **36**, 085105 (2009).
[4] R. K. Gupta, in *Clusters in Nuclei*, Vol. I, edited by C. Beck, Lecture Notes in Physics, Vol. 818 (Springer, Heidelberg, 2010), p. 223, and earlier references therein.
[5] E. T. Mirgule, D. R. Chakrabarty, V. M. Datar, S. Kumar, A. Mitra, V. Nanal, and P. C. Rout, Phys. Rev. C **82**, 064608 (2010).
[6] R. K. Gupta, M. Balasubramaniam, R. Kumar, N. Singh, M. Manhas, and W. Greiner, J. Phys. G: Nucl. Part. Phys. **31**, 631 (2005).
[7] R. K. Gupta, M. Manhas, and W. Greiner, Phys. Rev. C **73**, 054307 (2006).
[8] M. Bansal and R. K. Gupta, Rom. Journ. Phys. **57**, 18 (2012).
[9] P. Möller, J. R. Nix, W. D. Myers, and W. J. Swiatecki, At. Nucl. Data Tables **59**, 185 (1995).
[10] G. Audi and A. H. Wapstra, Nucl. Phys. A **595**, 4 (1995).
[11] S. K. Patra (private communication).
[12] S. Chopra, M. Bansal, M. K. Sharma, and R. K. Gupta, in *Proceedings of the Department of Atomic Energy (DAE) Symposium on Nuclear Physics* (2012), Vol. 57, p. 524, http://www.sympnp.org/proceedings/.
[13] S. Chopra and R. K. Gupta, in Proceedings of the 7th Chandigarh Science Congress, Chandigarh (CHASCON2013), March 1–3, 2013 (unpublished).
[14] R. Kumar, M. Bansal, S. K. Arun, and R. K. Gupta, Phys. Rev. C **80**, 034618 (2009).
[15] R. K. Gupta, M. Balasubramaniam, C. Mazzocchi, M. La Commara, and W. Scheid, Phys. Rev. C **65**, 024601 (2002).
[16] R. K. Gupta, R. Kumar, N. K. Dhiman, M. Balasubramaniam, W. Scheid, and C. Beck, Phys. Rev. C **68**, 014610 (2003).
[17] M. Balasubramaniam, R. Kumar, R. K. Gupta, C. Beck, and W. Scheid, J. Phys. G: Nucl. Part. Phys. **29**, 2703 (2003).
[18] G. Royer and J. Mignen, J. Phys. G: Nucl. Part. Phys. **18**, 1781 (1992).
[19] H. S. Khosla, S. S. Malik, and R. K. Gupta, Nucl. Phys. A **513**, 115 (1990).
[20] S. Kumar and R. K. Gupta, Phys. Rev. C **55**, 218 (1997).
[21] R. K. Gupta, S. Kumar, and W. Scheid, Int. J. Mod. Phys. E **6**, 259 (1997).
[22] T. Matsuse, C. Beck, R. Nouicer, and D. Mahboub, Phys. Rev. C **55**, 1380 (1997).
[23] S. J. Sanders, Phys. Rev. C **44**, 2676 (1991).
[24] S. J. Sanders, D. G. Kovar, B. B. Back, C. Beck, D. J. Henderson, R. V. F. Janssens, T. F. Wang, and B. D. Wilkins, Phys. Rev. C **40**, 2091 (1989).
[25] N. J. Davidson, S. S. Hsiao, J. Markram, H. G. Miller, and Y. Tzeng, Nucl. Phys. A **570**, 61c (1994).
[26] W. Myers and W. J. Swiatecki, Nucl. Phys. **81**, 1 (1966).
[27] A. S. Jensen and J. Damgaard, Nucl. Phys. A **203**, 578 (1973).
[28] B. B. Singh, M. K. Sharma, and R. K. Gupta, Phys. Rev. C **77**, 054613 (2008).
[29] R. K. Gupta, Niyti, M. Manhas, S. Hofmann, and W. Greiner, Int. J. Mod. Phys. E **18**, 601 (2009); R. K. Gupta, Niyti, M. Manhas, and W. Greiner, J. Phys. G: Nucl. Part. Phys. **36**, 115105 (2009).
[30] R. K. Gupta, S. Kumar, M. Balasubramaniam, G. Münzenberg, and W. Scheid, J. Phys. G: Nucl. Part. Phys. **28**, 699 (2002).
[31] R. K. Gupta, M. Balasubramaniam, S. Kumar, S. K. Patra, G. Münzenberg, and W. Greiner, J. Phys. G: Nucl. Part. Phys. **32**, 565 (2006).
[32] P. G. Hansen and B. Jonson, Europhys. Lett. **4**, 409 (1987).
[33] I. J. Thompson and J. S. Vaagen, in *Heavy Elements and Related New Phenomena*, Vol. II, edited by W. Greiner and R. K. Gupta (World Scientific, Singapore, 1999), p. 976.
[34] K. Ieki, A. Galonsky, D. Sackett, J. J. Kruse, W. G. Lynch, D. J. Morrissey, N. A. Orr, B. M. Sherrill, J. A. Winger, F. Deak, A. Horvath, A. Kiss, Z. Seres, J. J. Kolata, R. E. Warner, and D. L. Humphrey, Phys. Rev. C **54**, 1589 (1996).
[35] E. Sauvan *et al*., Phys. Rev. Lett. **87**, 042501 (2001).
[36] H. Kröger and W. Scheid, J. Phys. G **6**, L85 (1980).
[37] R. K. Gupta, in *Proceedings of the 5th International Conference on Nuclear Reaction Mechanisms, Varenna, Italy*, edited by E. Gadioli (Ricerca Scintifica Educazione Permanente, Milano, Italy) (Cooperative Libraria Universitaria del Politecnico, 1988), p. 416.
[38] S. S. Malik and R. K. Gupta, Phys. Rev. C **39**, 1992 (1989).
[39] S. J. Sanders, D. G. Kovar, B. B. Back, C. Beck, B. K. Dichter, D. Henderson, R. V. F. Janssens, J. G. Keller, S. Kaufman, T.-F. Wang, B. Wilkins, and F. Videbaek, Phys. Rev. Lett. **59**, 2856 (1987).
[40] R. K. Gupta, M. Balasubramaniam, R. Kumar, D. Singh, C. Beck, and W. Greiner, Phys. Rev. C **71**, 014601 (2005).
[41] R. Kumar, M. K. Sharma, and R. K. Gupta, Nucl. Phys. A **870-871**, 42 (2011).
[42] M. K. Sharma, S. Kanwar, G. Sawhney, and R. K. Gupta, Phys. Rev. C **85**, 064602 (2012).